

Orbital eccentricity growth through disc–companion tidal interaction

J. C. B. Papaloizou, R. P. Nelson, and F. Masset

Astronomy Unit, Queen Mary & Westfield College, Mile End Rd, London E1 4NS, UK

Received 8 June 2000 / Accepted 15 November 2000

Abstract. We investigate the driving of orbital eccentricity of giant protoplanets and brown dwarfs through disc–companion tidal interactions by means of two dimensional numerical simulations. We consider disc models that are thought to be typical of protostellar discs during the planet forming epoch, with characteristic surface densities similar to standard minimum mass solar nebula models. We consider companions, ranging in mass between 1 and 30 Jupiter masses M_J , that are initially embedded within the discs on circular orbits about a central solar mass. We find that a transition in orbital behaviour occurs at a mass in the range 10–20 M_J . For low mass planetary companions, we find that the orbit remains essentially circular. However, for companion masses $\gtrsim 20 M_J$, we find that non steady behaviour of the orbit occurs, characterised by a growth in eccentricity to values of $0.1 \lesssim e \lesssim 0.25$. Analysis of the disc response to the presence of a perturbing companion indicates that for the higher masses, the inner parts of the disc that lie exterior to the companion orbit become eccentric through an instability driven by the coupling of an initially small disc eccentricity to the companion’s tidal potential. This coupling leads to the excitation of an $m = 2$ spiral wave at the 1:3 outer eccentric Lindblad resonance, which transports angular momentum outwards, leading to a growth of the disc eccentricity. The interaction of the companion with this eccentric disc, and the driving produced by direct resonant wave excitation at the 1:3 resonance, can lead to the growth of orbital eccentricity, with the driving provided by the eccentric disc being the stronger. Eccentricity growth occurs when the tidally induced gap width is such that eccentricity damping caused by corotating Lindblad resonances is inoperative. These simulations indicate that for standard disc models, gaps become wide enough for the 1:3 resonance to dominate, such that the transition from circular orbits can occur, only for masses in the brown dwarf range. However, the transition mass might be reduced into the range for extrasolar planets if the disc viscosity is significantly lower enabling wider gaps to occur for these masses. Another possibility is that an eccentric disc is produced by an alternative mechanism, such as viscous overstability resulting in a slowly precessing non axisymmetric mass distribution. A large eccentricity in a planet orbit contained within an inner cavity might then be produced.

Key words. accretion, accretion disks – methods: numerical – stars: planetary systems

1. Introduction

Disc–companion interactions are important in a variety of astrophysical contexts ranging from orbital evolution, tidal interaction, and accretion in close binary systems (e.g. Lin & Papaloizou 1979; Artymowicz & Lubow 1994; Papaloizou & Terquem 1995; Larwood & Papaloizou 1997) to the evolution of black hole binary pairs in active galaxies (Begelman et al. 1980; Ivanov et al. 1999).

The recent discovery of a number of extrasolar giant planets orbiting around nearby solar–type stars (Marcy & Butler 1998, 2000) has stimulated renewed interest in the theory of planet formation and disc–companion interaction. These planetary objects have

masses, m_p , that are comparable to that of Jupiter ($0.25 M_J \lesssim m_p \lesssim 11 M_J$), have orbital semi-major axes in the range $0.03 \text{ AU} \lesssim a \lesssim 2.5 \text{ AU}$, and orbital eccentricities in the range $0.0 \lesssim e \lesssim 0.67$ (Marcy & Butler 2000). Explaining these data is one of the major challenges faced by planet formation theory.

The presence of the brown dwarf Gliese 229B with mass $\sim 45 M_J$ in a binary system indicates the potential existence of a separate population, at the one percent incidence level, of brown dwarfs (Oppenheimer et al. 2000) which could also form from discs, possibly through a different mechanism to that for extrasolar planets.

Recent simulations of protoplanets in the observed mass range (Kley 1999; Bryden et al. 1999; Lubow et al. 1999) interacting with a disc with parameters thought to be typical of protoplanetary discs, indicate gap formation

Send offprint requests to: R. P. Nelson,
e-mail: R.P.Nelson@qmw.ac.uk

and upper mass limit consistent with the observations. In addition simulations by Nelson et al. (2000) (hereafter NPMK) which allowed the protoplanet orbit to change found inward migration on near circular orbits leaving the observed eccentricities of extrasolar planets unexplained.

However, previous discussions of this problem (Artymowicz 1992; Lin & Papaloizou 1993a) have indicated that orbital eccentricity might be driven by disc-companion interactions. This might be expected from the general theory of tidal interaction. Jeffreys (1961) showed that a body in circular orbit around a rapidly rotating central object could have an instability driving orbital eccentricity. A similar instability might be expected for a body orbiting inside a rotating disc. In this case resonant wave excitation at the inner and outer eccentric Lindblad resonances leads to the excitation of eccentricity. However, a sufficiently wide gap is required to exclude coorbital and near coorbital disc material which would damp the eccentricity through coorbital Lindblad torques (Artymowicz 1993). Thus an eccentric instability would only be expected for a mass sufficiently large to clear a wide gap. The mass above which eccentric orbits might be excited is expected to be a function of the disc parameters.

Determination of this mass is important for the theory of disc-companion interactions and its implications for binary systems and the formation theory of planets and brown dwarfs. We find that the transition to an eccentric orbit can be linked to the driving of an eccentric disc, and it appears that the interaction between the companion and this disc eccentricity produces eccentricity driving that moderately exceeds that due to direct resonant wave excitation at the 1:3 outer eccentric Lindblad resonance discussed above. As the behaviour of the disc then also has a transition, different predictions for the mass spectrum and orbital distribution of more massive objects above the transition mass may result.

In this paper we investigate the driving of orbital eccentricity of giant protoplanets and brown dwarfs through disc-companion tidal interactions by means of two dimensional numerical simulations. We examined the evolution of companions ranging in mass between 1 and 30 M_J orbiting within protoplanetary discs about a central solar mass. For standard parameters, we find the transition to eccentric orbits occurs for companion masses that are greater than $\sim 20 M_J$.

In these cases the inner disc has accreted onto the central star. The inner parts of the disc that lie exterior to the companion orbit were found to become eccentric. This latter process is associated with the excitation of a $m = 2$ spiral wave at the 1:3 outer eccentric Lindblad resonance. This effect has a counterpart in the modelling of discs in Cataclysmic binaries. Here, in the lower companion mass range, an eccentric circumprimary disc has been seen (Whitehurst 1988; Hirose & Osaki 1990; Lubow 1991). This in turn is related to the excitation of a $m = 2$ spiral wave at the 3:1 inner eccentric Lindblad resonance, as described by Lubow (1991).

Our present results indicate eccentric orbits only for masses in the brown dwarf range. However, the transition mass might be reduced into the range for extrasolar planets if wider gaps or more extensive disc clearance occurs while allowing an outer eccentric disc to still exist.

The plan of the paper is as follows. In Sect. 2 we describe the physical model of the disc-companion system used. In Sect. 3 we describe the numerical methods. In Sect. 4 we present the numerical results which indicate the transition from circular companion orbit to eccentric companion orbit together with an eccentric outer disc for companion masses exceeding $\sim 20 M_J$. In Sect. 5 we give a simple analytic model illustrating how the eccentricity can be driven both in the companion orbit and exterior disc by an instability operating through density wave excitation at the outer 1:3 Lindblad resonance leading to a pattern rotating with $1/2$ the companion orbital frequency as seen in the numerical calculations. A similar analysis for the driving of eccentricity in circumstellar discs, but with fixed circular companion orbit, is discussed in Lubow (1991). Finally in Sect. 6 we discuss our results and speculate on how eccentric discs might produce eccentric orbits for masses in the planetary range.

2. The physical model

We solve the time dependent evolution equations for a system composed of a primary star, small mass companion, and viscous disc. The equations of motion and numerical procedures adopted are described in NPMK. For the sake of brevity we refer the reader to that paper for details.

We work with flat 2-dimensional disc models. In a cylindrical coordinate system (r, φ, z) centred on the central star, the disc rotation axis and the central star-companion object orbital angular momentum vectors are in the z direction. The equations of motion that describe the disc are the vertically integrated Navier-Stokes equations. The disc evolves in the combined gravitational field of the star and companion, and as a result of pressure and viscous forces. The star-companion orbit evolves under their mutual gravitational interaction and the gravitational field of the disc. For the calculations reported here, the companion gravitational potential was taken to be that of a softened point mass with softening parameter equal to $0.4r_L$, r_L being the Roche lobe radius. As with similar cases dealt with in NPMK, the companion was not permitted to accrete mass but could maintain a static atmosphere.

We use a locally isothermal equation of state, and prescribe the local sound speed $c_s = (H/r)v_K$ to be such that the disc aspect ratio $H/r = 0.05$ throughout the disc, $v_K = r\Omega_K$ being the Keplerian velocity. Thus the disc Mach number is 20 everywhere. We employ a constant value of the kinematic viscosity $\nu = 10^{-5}$ in dimensionless units (described below). The assumption implicit within this formalism is that the process that causes angular momentum transport in astrophysical discs may be modeled simply using an anomalous viscosity coefficient

in the Navier–Stokes equations, even though it probably arises through complicated processes such as MHD turbulence generated by the Balbus–Hawley instability (Balbus & Hawley 1991, 1998).

For computational convenience we adopt dimensionless units. The unit of mass is taken to be the sum of the mass of the central star (M_*) and companion (M_p). The unit of length is taken to be the initial orbital radius of the companion, r_p . The gravitational constant $G = 1$, so that the natural unit of time becomes

$$P_0/(2\pi) = \omega^{-1} = \sqrt{\frac{r_p^3}{G(M_* + M_p)}},$$

with P_0 being the initial orbital period of the binary, which in all cases was initiated on a circular orbit.

2.1. Initial conditions

The disc models used in all simulations had uniform surface density, Σ , with an imposed taper near the disc edge, initially. The value of Σ was chosen such that when $M_* = 1 M_\odot$, there exists the equivalent of 2 Jupiter masses (M_J) in the disc interior to the initial orbital radius of the companion. Then $\Sigma = 6 \cdot 10^{-4}$ in our dimensionless units.

Different mass ratios between the companion and the central star $q = M_p/M_*$, were considered, such that $10^{-3} \leq q \leq 0.03$. For $M_* = 1 M_\odot$, the lower end of this range corresponds to a Jupiter mass protoplanet and the upper end to a Brown Dwarf of mass $30 M_J$. The inner radius of the disc was located at $r = 0.4$ and the outer radius at $r = 6$.

2.2. Boundary conditions

Since material in a viscous accretion disc will naturally flow onto the central star, an outflow condition was applied at the inner boundary. The outer boundary condition was the same as that described in NPMK.

3. Hydrodynamic codes

The calculations presented here were performed with the three dimensional MHD code NIRVANA (here adapted to 2D) that has been described in depth elsewhere (Ziegler & Yorke 1997). Viscous forces have been added as described by Kley (1998).

In each case the equations are solved using a finite difference scheme on a discretised computational domain containing $N_r \times N_\phi$ grid cells, where the grid spacing in the (r, ϕ) coordinates is uniform.

For the calculations presented here and listed in Table 1, no accretion onto the companion was allowed and three different resolutions have been used. The run with $q = 10^{-3}$, listed as N1 in Table 1 used $N_r = 130$ and $N_\phi = 384$. The other lower resolution runs used $N_r = 200$ and $N_\phi = 200$. One higher resolution run used $N_r = 400$

Table 1. This table lists the label given to each simulation, the resolution used for each calculation ($N_r \times N_\phi$), the companion–star mass ratio, and whether strong eccentricity growth was observed

Run	Resolution	q	e growth?
N1	130×384	10^{-3}	No
N2	200×200	0.01	Yes
N3	200×200	0.02	Yes
N4	200×200	0.025	Yes
N5	200×200	0.03	Yes
N6	400×400	0.03	Yes

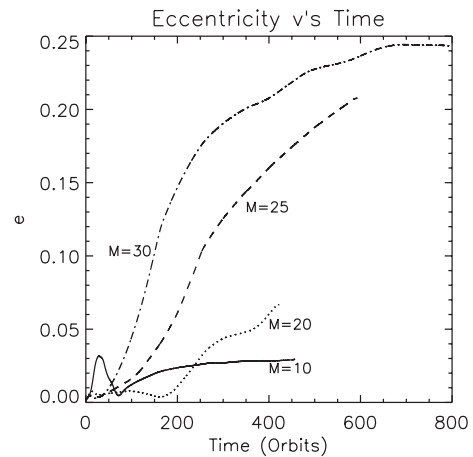


Fig. 1. This figure shows the evolution of the eccentricity versus time (measured in units of P_0) for the calculations, N2, N3, N4, N5 listed in Table 1. The lines corresponding to each companion of different mass are indicated on the figure in units of M_J

and $N_\phi = 400$. The numerical method is based on the monotonic transport algorithm of Van Leer (1977), leading to the global conservation of mass and angular momentum. The evolution of the companion orbit was computed using a standard leapfrog integrator.

NIRVANA has been applied to a number of different problems including that of an accreting protoplanet embedded in a protostellar disc (NPMK). It was found to give results that are very similar to those obtained with other finite difference codes including FARGO (described in Masset 2000) and RH2D (described in Kley 1999).

In order to establish the reliability of the numerical results, simulations were also performed using an alternative code based on the FARGO fast advection method (see Masset 2000, NPMK). In this scheme, which is able to operate with longer time steps than NIRVANA, a fourth-order Runge Kutta scheme was used as orbit integrator. Results obtained with the two codes were very similar.

4. Numerical calculations

Recent simulations of protoplanets with $0.001 < q < 0.01$, interacting with discs with physical parameters similar to

those adopted here, being thought to be appropriate to protoplanetary discs, have been carried out by Bryden et al. (1999), Kley (1999), and Lubow et al. (1999). Fixed circular orbits were assumed. It was found that a gap was formed that deepened and widened with increasing q . The disc interior to the orbit accreted onto the central star forming an inner cavity. Subsequent work by NPMK which allowed the orbit to evolve found that it remained essentially circular while migrating towards the central star.

We remark that Artymowicz (1992) indicated that orbital eccentricity growth might occur for sufficiently large $q \sim 0.01$, while Lin & Papaloizou (1993a) argued that for sufficiently wide gaps, eccentricity growth could be induced by interaction at the 1:3 resonance in the outer disc and the 3:1 resonance in the inner disc. As the latter is absent in the work presented here, only the 1:3 resonance in the outer disc will concern us.

The aim of the work presented here is to examine for what value of the companion–star mass ratio, if any, eccentricity growth of the companion orbit is induced by its interaction with the disc model that we assume. Should it occur, we wish to understand the dominant mechanism by which growth occurs and in particular whether the 1:3 resonance is involved.

The numerical calculations are summarised in Table 1. The case of $q = 10^{-3}$ was considered in some detail in NPMK. The planet/companion in this case was found to migrate in towards the central star on a time scale given by the viscous evolution time at the initial position of the planet (also see Lin & Papaloizou 1986) remaining on an essentially *circular* orbit. We will not give further discussion here on this case, since eccentricity growth was not observed.

The evolution of the eccentricity for the remaining cases listed in Table 1 is shown in Fig. 1. It is apparent from this figure that strong eccentricity growth occurs for mass ratios in the range $0.02 \lesssim q \lesssim 0.03$, with the strongest eccentricity growth being observed at the higher end of this range. From here onwards we will concentrate on describing the evolution of the $q = 0.03$ case.

A plot of the surface density evolution of run N5 described in Table 1 is shown in Fig. 2. The times corresponding to each panel are shown in the top right hand corner in units of P_0 . It can be seen that the disc interior to $r \sim 1.6$ is cleared out by the action of the companion tides on a relatively short time scale, and remains tidally truncated. Further evolution of the system leads to the formation of an eccentric outer disc, as may be observed in the third panel of Fig. 2. Figure 4 also shows the formation of an eccentric disc for a companion on a fixed circular orbit, and is described below. As the eccentricity of the companion increases beyond $e \gtrsim 0.1$, we observe that the disc response becomes non steady as the companion orbits between apocentre and pericentre. The evolution of the orbital radius of the companion and its eccentricity evolution (on both linear and log scales) are presented in Fig. 3. This figure shows that the eccentricity undergoes a period of rapid growth after a time of

$t \sim 50 P_0$. The logarithmic plot of e versus t shown in the second panel of this figure shows that the growth rate is initially constant (approximately), but then decreases as the system evolves beyond $t \sim 180 P_0$, indicating exponential growth during these early stages. Analysis of the torques being exerted on the companion between the times $50 \leq t \leq 150 P_0$ shows that the angular momentum is removed from the companion orbit and transferred to the disc as it approaches apocentre, leading to further growth of the orbital eccentricity. This, however, does not explain why the disc itself becomes eccentric during its early evolution. At a later time $t \sim 600 P_0$, the eccentricity reaches a maximum value ~ 0.25 . It subsequently enters into a sequence of cyclic variations, decreasing to small values at $t \sim 1500 P_0$, before increasing again. After the initial saturation the disc is always very eccentric and in contact with the companion at some orbital phases. This interaction of the companion with material with higher specific angular momentum causes the early net inward orbital migration to reverse such that the final semi-major axis at $t \sim 1900 P_0$ exceeds the initial one. But note that the details of this evolution depend on the manner in which the disc interacts with the companion and will be discussed by one of us in a future publication. Clearly the disc-companion interaction is very different in the brown dwarf regime from the planetary one.

In order to explore why the disc itself becomes eccentric, an identical simulation to N5 was performed, except that the companion was maintained on a fixed circular orbit. According to the discussion given below, non linear coupling between an eccentric disc mode (with small e) corresponding to an essentially time independent $m = 1$ pattern and the $m = 1$ component of the tidal potential and its disc response propagating with pattern speed equal to the orbital frequency, is expected to give rise to the excitation of an $m = 2$ spiral density wave emitted at the 1:3 outer eccentric Lindblad resonance. The pattern speed of this wave is half the orbital frequency. This wave can in turn couple back through the tidal potential to produce a time independent wave and associated potential with $m = 1$. The removal of angular momentum from the disc through such a potential will cause the disc eccentricity to increase. This is because no energy is removed along with the angular momentum, from the fluid orbits, so they cannot remain circular. If a wave with pattern speed equal to half the orbital frequency is present and launched from the 1:3 resonance, in a simulation with a companion on a fixed circular orbit, then it accounts naturally for the growth of disc eccentricity. Wave excitation is also expected to cause a growth in orbital eccentricity when that is present (see Lin & Papaloizou 1993a, and below). The excited wave is expected to have a pattern speed equal to $\omega_{1:3} = \omega/2$. Because the disc configuration changes to one in which the pattern rotation period has doubled, the instability produces a *period doubling* and so resembles a parametric instability.

A plot of the disc surface density for the run with the companion on a fixed circular orbit is shown in Fig. 4, in a

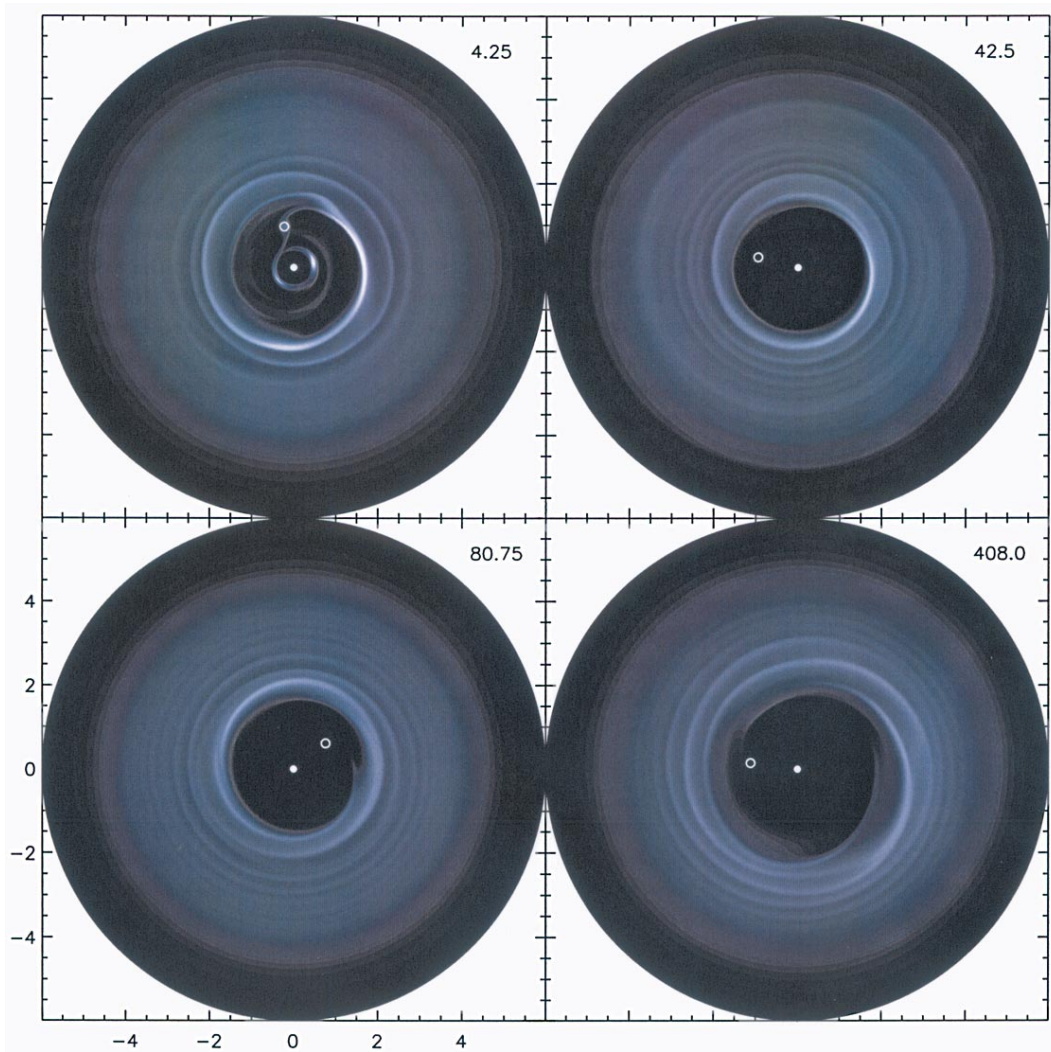


Fig. 2. This figure shows the evolution of the surface density profile of the disc in calculation N5 described in Table 1. The time, in units of P_0 , is shown at the top right hand corner of each panel. The initial clearing of a gap is shown in the first and second panel, and the growth of eccentricity of the disc interior to the 1:3 resonance (located at $r \simeq 2.08$) may be observed in the third panel. The fourth panel shows the disc at a later time when the companion has developed an eccentricity of $e \simeq 0.20$, and indicates that the behaviour of the disc becomes more complicated and unsteady during these later times

frame corotating with the orbit. The panels are separated by one third of the orbital period. The 1:2 outer Lindblad resonance is shown by the dotted line, and the eccentricity of the inner parts of the disc that lie just exterior to this resonance may be observed.

The disc surface density that resulted from the simulation in which the companion remained on a fixed circular orbit was Fourier transformed in azimuth, and the $m = 2$ component was examined. In line with our expectations, it was observed that once the inner disc was cleared of material, the presence of the $m = 2$ wave being launched from the 1:3 outer eccentric Lindblad resonance became apparent, travelling with a pattern speed $\omega/2$. This $m = 2$ component of Σ is plotted in Fig. 5 at different times during an orbit. Comparison between the first, fifth, and ninth panels, which are separated by an orbital period of the

star-companion system, show that the pattern does indeed repeat after this time interval. Comparison between panels separated by half an orbital period, such as the first and third, shows that the pattern does *not* repeat after half an orbital period. An $m = 2$ wave travelling with the orbital frequency ω would repeat after every half an orbital period. The fact that the $m = 2$ wave only repeats after every orbital period indicates that it is being excited at the 1:3 resonance (indicated by the dashed line in Fig. 5) with a pattern speed $\omega_{1:3} = \omega/2$. We conclude that a parametric instability is operating to excite this wave, giving rise to an eccentric disc. In calculation N5 where the star-companion orbit is able to evolve, the interaction between the companion and the eccentric disc leads to the growth of eccentricity of the companion orbit.

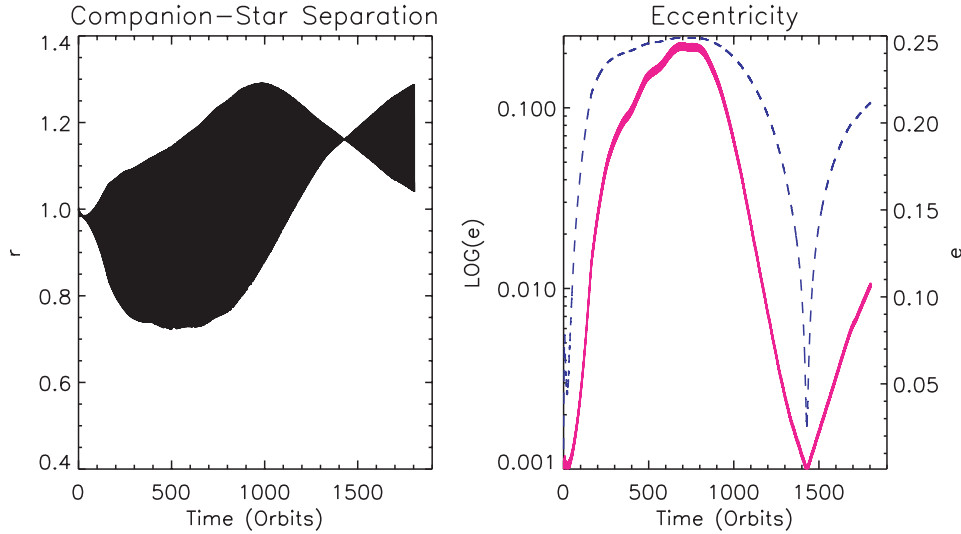


Fig. 3. This figure shows the evolution of the companion–star orbital separation as a function of time in the first panel, and the orbital eccentricity plotted as a log function (dotted line) and linear function (solid line) in the second panel. It is apparent that the eccentricity undergoes a period of rapid growth after $t \sim 50 P_0$. Between $t \sim 40$ and $100 P_0$, the growth is approximately exponential, as indicated by the plot of $\log(e)$ in the second panel which is close to being a straight line during these times. At later times, the growth rate decreases and the plots show a change of behaviour at $t \simeq 180 P_0$ when $e \simeq 0.12$. This change in the growth of e is accompanied by a change in the behaviour of the disc surface density response, which becomes very unsteady. This latter point was discussed in the caption of Fig. 2. On average there is net inward orbital migration until $t \sim 500 P_0$. After this time the eccentricity starts to decrease before increasing again in a cyclic variation. During these later phases the companion has contact with material with higher specific angular momentum from the eccentric disc. The interaction causes the inward migration to reverse

As described above, previous work on orbital eccentricity growth through disc–companion interactions indicated that direct resonant wave excitation at inner and outer eccentric Lindblad resonances should drive eccentricity, whereas interaction with material at corotating Lindblad resonances should cause it to damp (Artymowicz 1993; Lin & Papaloizou 1993a). In the simulations presented here, only the outer 1:3 resonance is important, and it is of interest to ask whether direct wave excitation at this resonance, or interaction with the disc eccentricity, is primarily responsible for the eccentricity growth of the companion orbit. To address this question, we performed simulations similar to run N5, but in which the surface density of the disc was Fourier analysed in azimuth. In these calculations the gravitational force of the disc acting on the star–companion orbit only included a contribution from an individual Fourier component ($m = 1, 2, 3$, or 4), though the full potential of the star–companion system acting on the disc was included. We expect that if the interaction of the companion with the disc eccentricity is dominant in driving the companion eccentricity then the calculation including only the $m = 1$ component of the disc gravitational potential will show more rapid growth of orbital eccentricity. Conversely, if resonant wave excitation of an $m = 2$ wave at the 1:3 resonance was primarily responsible, then the calculation including only the $m = 2$ component of the disc potential will show more rapid eccentricity growth. In fact, we find that the $m = 1$ run showed a moderately larger eccentricity growth than the

$m = 2$ run, suggesting that the orbital interaction with the eccentric disc produces the stronger growth. This conclusion is further suggested by the estimates of the eccentricity growth rates presented in Sect. 5.10.

The runs including only the $m = 3$ and $m = 4$ terms showed negligible eccentricity growth.

5. A simple analytic model

In order to help understand some of the simulation results described above, we consider a simplified model system of primary, orbiting companion and disc. We suppose the companion orbits inside a disc with truncated inner edge. We make the additional simplification that the central star remains fixed at the origin of the coordinate system. The disc itself is taken to be inviscid with a simple relation between vertically integrated pressure, P and surface density, Σ . Much of the complex nonlinear dynamics involving the balance between tides and viscosity determining the structure of the inner disc edge is thus omitted. However, enough content remains in order to display an instability leading to eccentricity growth in both disc and companion orbit, as well as the excitation of an outward propagating density wave with half the pattern speed. The existence of this has been described above.

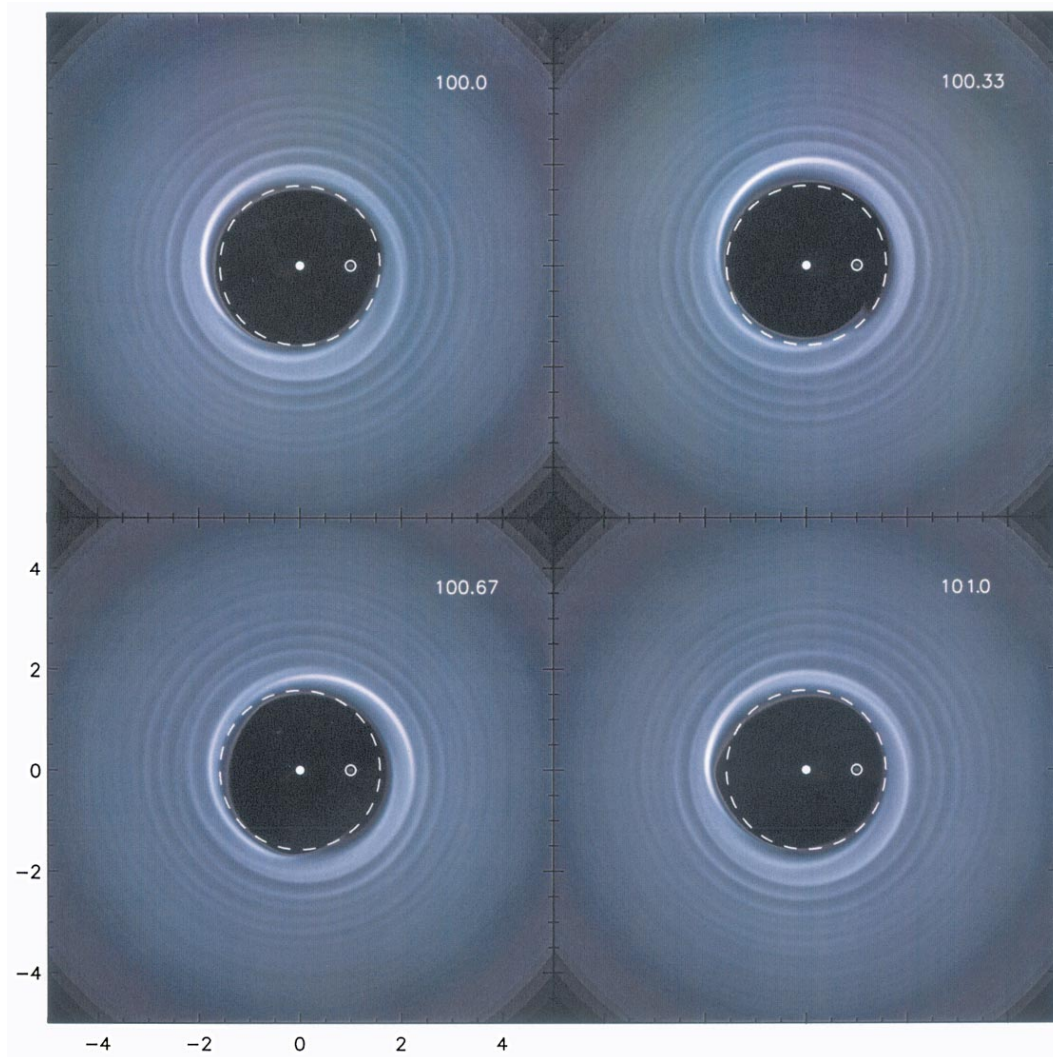


Fig. 4. This figure shows the eccentricity of the inner parts of the outer disc for a run in which the companion was maintained on a fixed circular orbit, with $M_p = 30 M_J$. The times of each panel are shown in the top right corner in units of the orbital period. The figure is plotted in a frame that is corotating with the binary orbit, and the dotted line indicates the position of the 1:2 outer Lindblad resonance

5.1. Slowly varying modes with $m = 1$

We are concerned here with the situation when the companion orbit becomes eccentric. In general it will precess with a period very much longer than the orbital period. In an inertial frame the time averaged orbit then appears as a perturbation of the unperturbed circular orbit with azimuthal mode number $m = 1$.

5.2. Secular perturbation theory

Because we are interested in modes that appear to change slowly in the inertial frame, we adopt the approach of secular perturbation theory. We thus perform a time average over an interval long compared to the orbital period but short compared to the orbital precession period.

The companion then acts gravitationally as if its mass were continuously distributed along its orbit with line

density inversely proportional to its speed. In an average sense it behaves like a continuous mass distribution and can be regarded as an infinitesimally thin annular extension of the disc. In this respect we suppose that we have a disc with well defined inner edge, interior to which there is a gap or hole in which the companion orbits. In the secular theory, we shall regard the companion as equivalent to an annular extension of the disc orbiting inside the gap and consider an eccentric companion orbit as a non axisymmetric perturbation of the initially axisymmetric combined disc-companion system. In this way an eccentric disc is produced also as comprising the normal mode. Good coupling results in eccentricities of comparable magnitudes in both components, while weak coupling enables them to exhibit eccentricities separately. The condition for good coupling is that the precession period induced in disc orbits by the companion and its own pressure and self-gravity be comparable to the precession period induced in

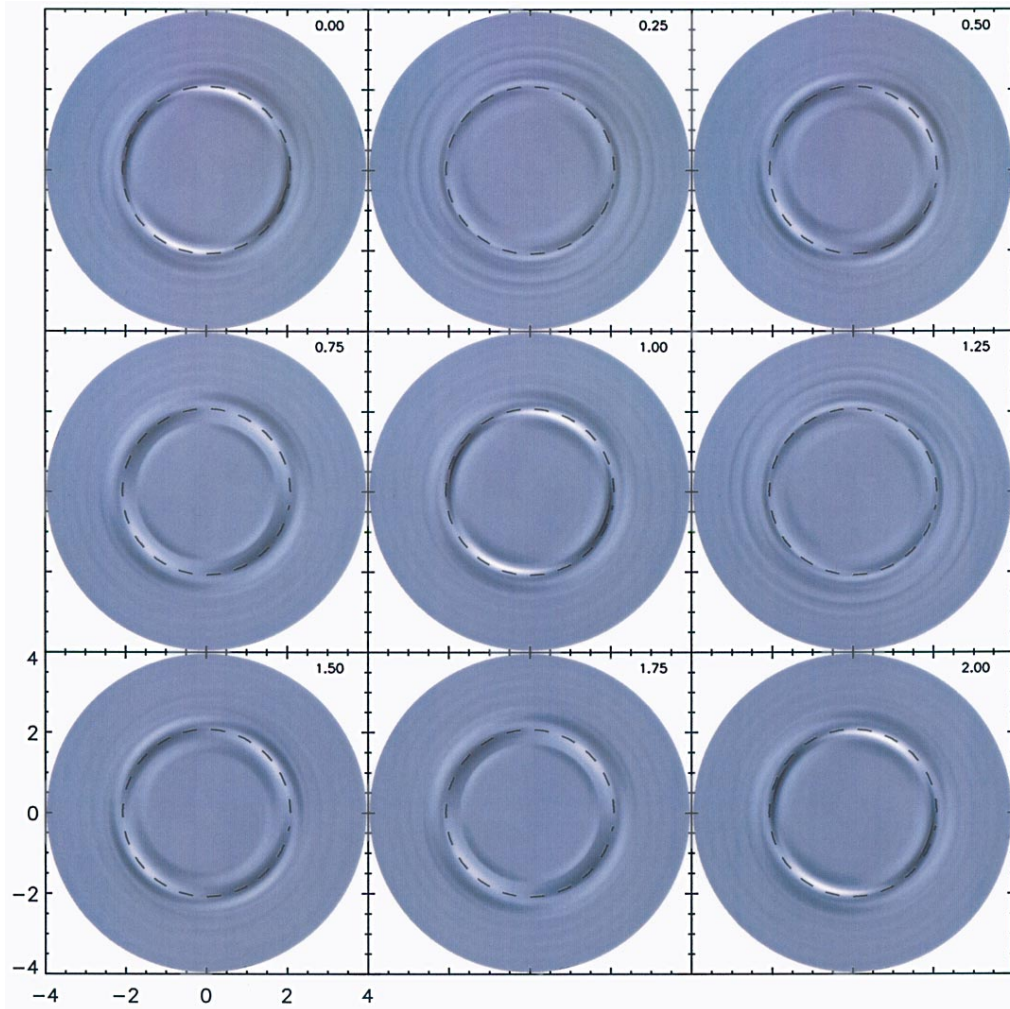


Fig. 5. This figure shows the evolution of the $m = 2$ component of the Fourier transform of the surface density, in the inertial frame, for the case of a $M_p = 30 M_{\text{Jupiter}}$ companion on a fixed circular orbit. The time elapsed when moving between the panels is shown in the top right hand corner, in units of P_0 , where we have arbitrarily denoted the time of the first panel to be $t = 0.0$. From the discussion in the text, it is expected that an $m = 2$ spiral density wave will be excited at the 1:3 outer eccentric Lindblad resonance, located at $r \simeq 2.08$ (shown by the dashed line), if the eccentricity growth of the disc arises because of a *period doubling* instability. This wave should have a pattern speed $\omega_{1:3} = \omega/2$. For an $m = 2$ feature, the observed pattern should repeat every P_0 , but not every $P_0/2$ (as would be the case if the wave had a frequency ω). Comparing the first and fifth panels, it is apparent that the $m = 2$ pattern does indeed repeat after every P_0 . Comparing the first and third panels, it is obvious that the $m = 2$ feature does not repeat every $P_0/2$

the companion orbit by the disc. This is met when the disc mass, M_d , contained in a radial scale comparable to the gap radius (or 1:3 resonance radius as taken below) is comparable to the mass of the companion. When these masses are very different, the situation will favour either an eccentric companion orbit or an eccentric disc.

This occurs because the slowly precessing nonaxisymmetric pattern in the disc makes it behave similarly to a planet of mass M_d . From standard secular perturbation theory (Brouwer & Clemence 1961) eccentricity is freely exchanged between this planet and the companion when their orbital angular momenta are comparable, a situation that occurs here when the masses are comparable.

5.3. Negative angular momentum modes

The slowly varying $m = 1$ modes described above are found to be negative angular momentum modes. This means that if they induce an angular momentum transfer to outer disc material from the region where they are located, they will grow unstably. Within the framework of secular perturbation theory of an initially axisymmetric disc this does not occur. However, if the high frequency components of the companion potential are now allowed to act, their coupling with the $m = 1$ secular mode induces an angular momentum loss and hence growth. This occurs through the coupling of the $m = 1$ low frequency mode with an $m = 1$ potential component with pattern speed equal to the orbital frequency. This produces a

forcing potential with $m = 2$ and pattern speed one half the orbital frequency. As we shall see this can produce a density wave resonantly excited at the 1:3 resonance located at $r = 2.08r_p$, r_p being the companion semi-major axis, provided that resonance is contained within the disc, and hence mode growth. A favourable situation occurs when the gap or inner hole is large enough that possibly stabilizing corotation resonances are absent (Goldreich & Tremaine 1980; Artymowicz 1993; Lin & Papaloizou 1993a).

When growth occurs we find two limiting cases. When the companion mass dominates that of the disc, an eccentric disc is produced. This situation is illustrated by our run in which the companion was maintained on a fixed circular orbit. In the opposite case, an eccentric companion orbit is expected as has been previously discussed by e.g. Artymowicz (1992) and Lin & Papaloizou (1993a). In the intermediate case eccentricities in both components are produced.

5.4. Slowly varying modes involving disc and companion

We consider linear perturbations of a two dimensional flat axisymmetric disc and time averaged planet. The dependence on time, t , and azimuthal angle, φ , is taken to be through a factor $\exp i(m\varphi + \sigma t)$ henceforth taken as read. Here the azimuthal mode number $m = 1$ and the mode frequency σ is such that $|\sigma| \ll \Omega$, where Ω is the angular velocity in the unperturbed disc where the unperturbed surface density is Σ .

The Lagrangian displacement $\xi = (\xi_r, \xi_\varphi)$ obeys the perturbed equations of motion

$$-(\sigma + \Omega)^2 \xi_r - 2i\Omega(\sigma + \Omega)\xi_\varphi + 2r\Omega \frac{d\Omega}{dr} \xi_r = -\frac{\partial W}{\partial r}. \quad (1)$$

$$-(\sigma + \Omega)^2 \xi_\varphi + 2i\Omega(\sigma + \Omega)\xi_r = -\frac{iW}{r}. \quad (2)$$

Equations (1) and (2) can be combined to give

$$(-(\sigma + \Omega)^2 + \kappa^2) \xi_r = -\frac{\partial W}{\partial r} - \frac{2\Omega W}{r(\sigma + \Omega)}. \quad (3)$$

Here $W = \Sigma' c^2 / \Sigma + \Psi'$, where Σ' and Ψ' are the surface density and gravitational potential perturbations respectively. The vertically integrated pressure P is assumed to be a function of Σ , $c^2 = dP/d\Sigma$ is the square of the sound speed, and $\kappa^2 = 2\Omega r^{-1} d(r^2 \Omega)/dr$ is the square of the epicyclic frequency.

The perturbation to the gravitational potential may be written (temporarily restoring the φ dependence)

$$\Psi' = G \int \frac{\nabla \cdot (\Sigma(\mathbf{r}') \xi(\mathbf{r}'))}{|\mathbf{r} - \mathbf{r}'|} r' dr' d\varphi', \quad (4)$$

where this and similar integrals are taken over the active mass distribution.

We may apply (4) to both the distributed disc mass and the separated, time averaged, but initially radially localized companion mass for which

$$\Sigma = \frac{M_p \delta(r - r_p)}{2\pi r_p}. \quad (5)$$

Here δ denotes a delta function and M_p the companion mass.

Before so doing, we use the fact that $|\sigma|/\Omega$ is small to make some simplifications. In this limit and for a thin disc for which forces due to internal pressure and self-gravity are small, Eq. (2) becomes

$$\xi_\varphi = 2i\xi_r, \quad (6)$$

which is the limiting form for purely epicyclic motion. We use this to evaluate the pressure and self-gravity terms on the right hand side of (3). The error in doing this, for a gravitationally stable disc, is measured by the greater of $|\sigma|/\Omega$ and H/r , where H is the semi-thickness of the disc.

Then we have

$$\Sigma' = -r \frac{d(r^{-1} \Sigma \xi_r)}{dr}. \quad (7)$$

Equation (4) can then be written

$$\Psi' = G \int \left(r \frac{d(r^{-1} \Sigma \xi_r)}{dr} \right)_{r=r'} K(r, r') r' dr', \quad (8)$$

with

$$K_m(r, r') = \int_0^{2\pi} \frac{\cos(m\varphi)}{\sqrt{(r^2 + r'^2 - 2rr' \cos(\varphi))}} d\varphi, \quad (9)$$

and noting that for $m = 1$ we shall drop the subscript from $K_m(r, r')$, thus $K_1(r, r') \equiv K(r, r')$.

We finally obtain a normal mode equation for ξ_r by using (8), and (7) in (3) in the form

$$2(\sigma + \omega_p) \Omega r \xi_r = -\frac{1}{r} \frac{d}{dr} \left(\frac{r^3 c^2}{\Sigma} \frac{d(r^{-1} \Sigma \xi_r)}{dr} \right) + \frac{1}{r} \frac{d(r^2 \Psi')}{dr}. \quad (10)$$

Here we have used the fact that $|\sigma|/\Omega \ll 1$, and the precession frequency $\omega_p = \Omega - \kappa$.

5.5. Disc and companion system

Although Eq. (10) applies to the joint disc and companion system, we shall separate the contributions to the potential from the companion and disc, writing

$$\Psi' = \Psi'_d + \Psi'_p, \quad (11)$$

where Ψ'_d , and Ψ'_p are the contributions from the disc and planet obtained from the appropriate surface density distributions respectively. Using (5), we find

$$\Psi'_p(r) = -\frac{GM_p \xi_r(r_p)}{2\pi r_p^2} \frac{\partial}{\partial r_p} (K(r, r_p) r_p^2). \quad (12)$$

Here the eccentricity of the companion orbit is related to the displacement by $e = \xi_r(r_p)/r_p$.

5.6. Disc modes

If we replace Ψ' in (10) by the disc contribution Ψ'_d only, we obtain an equation for the normal modes of the disc only. In fact under reasonable boundary conditions that ξ_r is well behaved at the inner boundary and vanishes at large distances, (10) gives a self-adjoint eigenvalue problem for the eigenvalue σ . The right hand side gives a self-adjoint operator with weight Σ . Denoting, the eigenvalues by σ_j , and corresponding eigenfunctions, ξ_r by u_j , $j = 1, 2, \dots$, we have the orthogonality condition

$$\int \Sigma \Omega r u_k^* u_j dr = N_j \delta_{kj}, \quad (13)$$

with this and later integrals being taken over the disc.

We comment that the eigenvalues are all real and the local dispersion relation associated with (10) is the low frequency limit of the well known relation for spiral density waves (Lin & Shu 1964)

$$2(\sigma + \omega_p) \Omega = -2\pi G \Sigma |k| + c^2 k^2, \quad (14)$$

where k is the radial wavenumber and of course $m = 1$. Each mode propagates with a prograde pattern speed $-\sigma_j$, which is also the precession frequency.

5.7. The effect of the companion

The effect of the companion may be incorporated by adding Ψ'_p into Ψ' in (10). Regarding the companion potential so added as giving an external forcing term, Eq. (10) may be solved using the standard method of eigenfunction expansion to give interior to the disc

$$\xi_r = - \sum_{j=1}^{\infty} \frac{u_j}{2N_j(\sigma - \sigma_j)} \int r^2 \Psi'_p \frac{d(r^{-1} \Sigma u_j^*)}{dr} dr. \quad (15)$$

5.8. Combined modes

Omitting the pressure term, Eq. (10) gives for the equation of motion of the companion

$$2[\sigma + \omega_p(r_p)] \Omega(r_p) \xi_r(r_p) = - \left[\frac{1}{r^2} \frac{d(r^2 \Psi'_d(r))}{dr} \right]_{r=r_p} \quad (16)$$

with

$$\Psi'_d(r) = -G \int \frac{\Sigma(r') \xi_r(r')}{r'} \frac{\partial}{\partial r'} (K(r, r') (r')^2) dr'. \quad (17)$$

Combining (16), (15) and (17) gives an equation for the eigenvalue σ for the joint normal mode in the form

$$[\sigma + \omega_p(r_p)] \Omega(r_p) = \sum_{j=1}^{\infty} \frac{|C_j|^2 M_p}{8\pi r_p^2 N_j (\sigma - \sigma_j)}, \quad (18)$$

with the coupling coefficient given by

$$C_j = G \int (r' r_p)^{-1} \Sigma(r') u_j(r') \frac{\partial^2}{\partial r' r_p} \times (K(r_p, r') (r' r_p)^2) dr'. \quad (19)$$

The schematic behaviour of the eigenvalues is that, when the coupling coefficient C_j is negligible, the solutions are $\sigma = \sigma_j$, $j = 1, 2, \dots$ and $\sigma = -\omega_p(r_p)$. In this case the companion and disc are decoupled and precess independently. In contrast when the coupling is non negligible the precession of companion orbit and disc are linked. One induces eccentricity in the other. To estimate when this occurs, one needs that $(|C_j|^2 M_p)/(8\pi r_p^2 N_j \Omega)$ be of the same order as the square of the difference in disc and companion orbit precession frequencies $(\omega_p + \sigma_j)^2$. If the companion and disc mutually induce eccentricity and precession, simple estimates, assuming there is a single radial scale length, indicate this requires that $M_d \sim M_p$ for good coupling.

We comment that although the gravity of the disc acting on both itself and the companion has been included in the above formalism, the self-interaction only affects the precise determination of the σ_j and u_j . The above discussion still applies if that is neglected, as long as the interaction with the companion is retained. This is the case for the simulations presented here.

5.9. Mode angular momentum

The effective angular momentum content in the joint mode can be evaluated using standard methods (e.g. Goodman & Ryu 1992; Lin & Papaloizou 1993b). For the low frequency modes considered here, we obtain after a straightforward calculation

$$\mathcal{J} = -\frac{1}{2} \int \Sigma |\xi_r|^2 \Omega r dr d\varphi, \quad (20)$$

where the integral is over the entire system.

We comment that, using (5), the contribution from the companion to \mathcal{J} is $\mathcal{J}_p = -1/2 M_p e^2 \sqrt{(GM_*) r_p}$. This is negative corresponding to a negative angular momentum mode and it is also minus the radial action. If angular momentum is drained from the mode, the companion orbit eccentricity and radial action grow. In general the total angular momentum content is

$$\mathcal{J} = -\frac{1}{2} M_p e^2 \sqrt{(GM_*) r_p} - \frac{1}{2} \int \Sigma |\xi_r|^2 \Omega r dr d\varphi, \quad (21)$$

where the second contribution now comes from the disc only, involving the radial component of the Lagrangian displacement $\xi_r \equiv er$ there.

5.10. Angular momentum loss due to resonant torques

The modes discussed above, in the time averaging approximation, do not lose angular momentum. However, only the time averaged potential due to the companion has been included. When the effects of the full potential

are included, additional perturbation of the disc occurs. This can lead to angular momentum loss through resonant torques (Goldreich & Tremaine 1978). In that case, the mode eccentricities grow and instability occurs.

The full potential due to the companion located at (r_p, φ_p) can be written

$$\Psi'_p = -\frac{GM_p}{\pi} \sum_{m=0}^{\infty} \frac{K_m(r, r_p) \cos m(\varphi - \varphi_p)}{(1 + \delta_{m0})}. \quad (22)$$

When the disc and companion orbit are eccentric, with small eccentricities, to evaluate the companion potential at the location of a perturbed fluid element in the disc, we set $r \rightarrow r + |\xi_r| \cos(\varphi)$, $\varphi \rightarrow \varphi - |\xi_\varphi| \sin(\varphi)/r$, $r_p \rightarrow r_p + er_p \cos(\omega t)$, $\varphi_p \rightarrow \omega t - 2e \sin(\omega t)$. Here, arbitrary phases are chosen such that all ellipses have apsidal lines aligned at $\varphi = t = 0$, consistently with the joint mode. The orbital frequency is ω and we have neglected the small precession frequency. The simulations suggest an alignment such the eccentricities of the disc and orbit are of opposite sign. In this case the disc pericentre is closest to the orbital apocentre. The contribution to the companion potential that is first order in the eccentricities Ψ'_{pe} is given by

$$\begin{aligned} \frac{\Psi'_{pe}}{GM_p} = & - \sum_{m=0}^{\infty} \frac{\cos m\beta}{\pi(1 + \delta_{m0})} \\ & \times \left(|\xi_r| \cos \varphi \frac{\partial}{\partial r} + er_p \cos \omega t \frac{\partial}{\partial r_p} \right) K_m(r, r_p) \\ & + \sum_{m=1}^{\infty} m K_m(r, r_p) \frac{\sin m\beta}{\pi} \\ & \times [-|\xi_\varphi| \sin \varphi / r + 2e \sin(\omega t)], \end{aligned} \quad (23)$$

where $\beta = \varphi - \omega t$.

We comment that for zero eccentricities, all time dependent components of the companion potential have pattern speed ω . In the outer disc, there are possible outer Lindblad resonances where $\Omega = m\omega/(m+1)$, $m = 1, 2, \dots$. However, as the inner edge approaches the 1:2 resonance, only the resonance with $m = 1$ remains eventually. When eccentricities are included, contributions occur in (23) with pattern speeds $(m-1)\omega/m$, $m = 2, 3, \dots$. The outer Lindblad resonances associated with these are at $\Omega = (m-1)\omega/(m+1)$. For $m = 2$, this gives the smallest value of $\Omega = \omega/3$ which occurs at the 1:3 resonance. The corresponding pattern speed of the resonant forcing is $\omega/2$.

As the material at the outer Lindblad resonance rotates more slowly than the pattern speed, resonant torques cause angular momentum loss leading to eccentricity growth of the joint disc-companion system. For discs with inner edges approaching the 1:2 resonance such that the disc surface density becomes depressed there, potentially damping corotation torques (Goldreich & Tremaine 1980) and coorbital Lindblad torques (Artymowicz 1993) are weakened. Here we shall assume that only the 1:3 resonance needs to be considered.

The resonant forcing occurs through terms produced by a nonlinear coupling between the secular $m = 1$ mode and disturbances with $m = 1$ moving with the orbital pattern speed ω . We begin by calculating the resonant forcing using (23) as a forcing potential on the unperturbed axisymmetric disc. However, it is important to note that not all the effective forcing terms are included in this way. They arise also by coupling between the secular $m = 1$ mode and the tidal distortion of the disc produced by the circular orbit tide propagating with a pattern speed ω . Evaluation of these is lengthy and depends on the detailed disc model which has here been simplified. Instead of such evaluation, we replace the disc eccentricity in (23) by \bar{e}_d to indicate additional forcing. Although such forcing is not necessarily through a potential, it can still be taken into account by defining a suitable \bar{e}_d which is proportional to the disc eccentricity amplitude (see Eq. [24]).

This procedure will enable eccentricity growth rates to be qualitatively discussed and estimated.

The component of (23) with pattern speed $\omega/2$, is then given by $\Psi'_{pe2}(r, r_p) \cos(2\varphi - \omega t)$, where

$$\begin{aligned} \frac{\pi \Psi'_{pe2}}{GM_p} = & -\bar{e}_d r \left(\frac{1}{2} \frac{\partial K(r, r_p)}{\partial r} - \frac{K(r, r_p)}{r} \right) \\ & - er_p \left(\frac{1}{2} \frac{\partial K_2(r, r_p)}{\partial r_p} + \frac{2K_2(r, r_p)}{r_p} \right). \end{aligned} \quad (24)$$

Here we have set $|\xi_r| = |\xi_\varphi|/2 = \bar{e}_d r$.

We calculate the rate of loss of angular momentum as a result of resonant torques using the torque formula of Goldreich & Tremaine (1978, 1980) to obtain

$$\frac{d\mathcal{J}}{dt} = -\frac{2\pi^2 r^2 \Sigma}{\omega^2} \left(\frac{\partial \Psi'_{pe2}}{\partial r} - \frac{4\Psi'_{pe2}}{r} \right)^2, \quad (25)$$

where r and the disc quantities are evaluated at the 1:3 resonance.

The angular momentum is transported outwards via a wave with pattern speed $\omega/2$. It has to be extracted from the $m = 1$ joint mode and the companion orbit which have combined together to give the resonant forcing.

Extraction from an eccentric companion orbit can occur directly through the excited $m = 2$ wave. Extraction from the $m = 1$ mode can occur through a recoupling of the $m = 2$ wave with the tidal potential with pattern speed ω , to produce a time independent forcing with $m = 1$. Similarly extraction from the orbit can occur through recoupling of the $m = 2$ wave to the $m = 1$ joint mode to produce an $m = 1$ disturbance with the circular orbit pattern speed ω .

If the resonantly excited $m = 2$ wave carries an angular momentum ΔJ , the associated energy is $\omega \Delta J/2$. If this energy is supplied by the circular orbit tide, then the angular momentum supplied along with it will be $\Delta J/2$, leaving $\Delta J/2$ to be extracted from the joint $m = 1$ mode.

The above discussion suggests the growth rate of this mode can be obtained by assuming half the resonantly induced angular momentum loss is extracted from it.

The growth rate of the combined mode is then estimated as

$$\gamma = \frac{1}{4\mathcal{J}} \frac{d\mathcal{J}}{dt}, \quad (26)$$

with

$$\mathcal{J} = -\frac{1}{2}M_{\text{p}}e^2\sqrt{(GM_*)r_{\text{p}}} - \frac{1}{2}\int\Sigma e_{\text{d}}^2r^3\Omega dr d\varphi. \quad (27)$$

Evaluating (25) we obtain

$$\begin{aligned} \frac{\gamma}{\omega} &= \frac{M_{\text{d}}M_{\text{p}}}{M_*^2} \left(\frac{r_{\text{p}}}{r}\right)^8 \\ &\times \frac{9\pi \left[(4\bar{e}_{\text{d}} - \frac{2r}{3}\frac{d\bar{e}_{\text{d}}}{dr})\frac{r}{r_{\text{p}}} - \frac{21}{4}e(1 + \frac{5}{7}(\frac{r_{\text{p}}}{r})^2) \right]^2}{\left[e^2 + \int 2\pi\Sigma e_{\text{d}}^2r^3\Omega dr / (M_{\text{p}}\omega r_{\text{p}}^2) \right]} \end{aligned} \quad (28)$$

where $M_{\text{d}} = \pi\Sigma r^2$.

Note that here we neglect any change in the companion semi-major axis due to the time dependent terms in the disc potential.

To set the magnitudes of typical growth rates, we first set the terms involving the disc eccentricity $e_{\text{d}}, \bar{e}_{\text{d}}$ to zero. We find from (28) that for the 1:3 resonance with $r = 2.08r_{\text{p}}$, $\gamma^{-1} = M_*^2/(19M_{\text{d}}M_{\text{p}})P_0$, with P_0 being the orbital period. Thus for $M_{\text{p}} = 2M_{\text{d}} = 0.03M_*$, here we allow a factor of two surface density enhancement above the initial value at the 1:3 resonance, we find a growth time ~ 120 companion orbital periods. This is comparable, but a factor of ~ 3 smaller, than the eccentricity growth rate obtained for calculation N5, and is consistent with the idea that the orbital eccentricity driving arises through effects due to both the orbital eccentricity itself and the eccentricity induced in the disc, the latter actually giving stronger effects.

We comment that for these parameters the disc and companion orbit eccentricities are likely to be coupled. This is because typically $M_{\text{d}} \sim M_{\text{p}}$. Then the precession frequency induced by the companion in externally orbiting disc matter is given by $\omega_{\text{p}} = 0.75\Omega(r)(r_{\text{p}}/r)^2(M_{\text{p}}/M_*)$. Similarly the precession frequency induced by the disc (assumed to have constant surface density) in the companion orbit is $\omega_{\text{p}} = \Omega(r_{\text{p}})(r_{\text{p}}/r)^3(M_{\text{d}}/M_*)$. These are comparable leading to the likely setting up of a joint mode. We comment that this condition is the same as requiring that the companion orbital angular momentum and the orbital angular momentum contained in M_{d} assumed in circular orbit be comparable.

Under the conditions of the simulations considered here, $M_{\text{d}} \sim M_{\text{p}}$. Then it is also likely that the radial action in the disc is comparable to that of the companion and so modifies the growth rate. However, as long as they are comparable our estimate is probably reasonable. Note that $\gamma^{-1} \propto M_*^2/(M_{\text{d}}M_{\text{p}})P_0$ as long as M_{p} is comparable to or less than M_{d} . If the companion mass dominates, so fixing it in a circular orbit, then $e = 0$, in (28) and $\gamma^{-1} \propto M_*^2/(M_{\text{p}}^2)P_0$, attaining a limiting value independent of the disc mass. Our simulation with fixed companion orbit indicates that the growth rate does not change very much as M_{d} is reduced significantly below M_{p} .

6. Discussion

In this paper we have investigated the driving of orbital eccentricity of giant protoplanets and brown dwarfs through disc-companion tidal interactions by means of two dimensional numerical simulations. Disc models thought to be typical of protostellar discs during the planet forming epoch, with characteristic surface densities similar to standard minimum mass solar nebula models were considered. We examined the evolution of companions ranging in mass between 1 and 30 M_{J} initially embedded within the discs on circular orbits. For low mass companions, typical of giant planets, we found, in agreement with our previous work (NPMK) that the orbit remains essentially circular. For companion masses that are greater than $\sim 20 M_{\text{J}}$, however, we found that a transition occurs, leading to a non steady behaviour of the companion orbit. This is characterised by a growth in eccentricity such that $0.1 \lesssim e \lesssim 0.25$.

The inner parts of the disc that lie exterior to the companion orbit become eccentric through an instability driven through the coupling of the non circular motions associated with a small disc eccentricity to the companion's tidal potential. This coupling leads to the excitation of an $m = 2$ spiral wave at the 1:3 outer eccentric Lindblad resonance, which transports angular momentum outwards. A similar picture of disc eccentricity driving for inner discs has been discussed by Lubow (1991) in the context of Cataclysmic Variables. As the disc eccentricity corresponds to a negative angular momentum mode, this angular momentum loss leads to a growth of the disc eccentricity. In addition to the effects of resonant wave excitation at the 1:3 resonance produced by the direct forcing of the companion in its eccentric orbit, the gravitational interaction of the companion with this eccentric disc leads to the growth of eccentricity of the companion orbit, where this latter effect is found to be moderately larger.

For a companion orbiting within a disc, the effects of the 1:3 resonance lead to growth of the eccentricity while the effects of corotation and coorbital Lindblad resonances lead to its damping (e.g. Artymowicz 1993; Ward & Hahn 2000). For a very wide gap or isolation of the companion from the disc material, the effects of the 1:3 resonance win and the eccentricity grows (Lin & Papaloizou 1993a).

However, our simulations indicate that for standard disc models, sufficient clearance due to the companion tides occurs only for masses in the brown dwarf range. However, the transition mass might be reduced into the range for extrasolar planets if the disc viscosity is significantly lower enabling wider gaps to occur. One can estimate the viscosity required by noting that the gap must extend out to the 1:2 resonance. For $\nu = 10^{-5}$ as adopted here the gap half width is ~ 0.2 for 1 M_{J} . To reach the 1:2 resonance this has to be three times larger. From Lin & Papaloizou (1993a) and Bryden et al. (1999), the tidal torque, which varies as the inverse cube of the gap width, is then reduced by a factor of 27. To prevent

the gap filling the viscosity would have to be reduced by at least the same factor requiring $\nu \leq 3 \cdot 10^{-7}$. This corresponds to the Shakura & Sunyaev (1973) viscosity parameter, $\alpha \leq 1.5 \cdot 10^{-4}$. Note that this is significantly smaller than values normally adopted for protostellar discs (e.g. Papaloizou & Terquem 1999).

We also found that when the angular momentum content of the disc material within a scale characteristic of the inner edge radius is comparable to that of the companion in a circular orbit, the eccentricity of the disc and companion are coupled. This behaviour occurs because the gravitational potential produced by the disc is similar to that of another companion in eccentric orbit. A coupling is then expected from standard secular perturbation theory. When the companion and disc masses are disparate, orbital eccentricity would be expected only for the smaller of the two.

Although the extrasolar planet mass range is too small (Marcy & Butler 2000) for eccentricity driving due to the 1:3 resonance assuming standard disc parameters, it is possible that it could be produced if the protoplanet orbits in a cavity with an eccentric external disc. This would require disc $m = 1$ modes to be excited by some other mechanism e.g. viscous overstability (Kato 1978; Papaloizou & Lin 1988). A slowly precessing non axisymmetric mass distribution would then be produced. A configuration like the one described above might be produced during the phase of disc clearance. There is observational evidence that this occurs on a 10^5 yr time scale working from the inside out (Shu et al. 1993). The precession period of the nonaxisymmetric mass distribution would be time variable and could potentially equal that of the inner protoplanet orbit at some stage. Because the average disc and protoplanet orbits would then maintain a fixed orientation, a large eccentricity in the protoplanet orbit can be produced by gravitational torques on the precession time scale. Notably the effect need not be correlated with the protoplanet mass. A mechanism operating on the same principle has been proposed by Ward et al. (1976) as a mechanism for producing the eccentricity of Mercury.

The precession frequency induced by the disc (assumed to have constant surface density) in the protoplanet orbit is $\omega_p = \Omega(r_p)(r_p/r)^3(M_d/M_*)$. For $r_p = 1$ au, $r = 10$ au, $M_d/M_* \sim 0.01$, this gives a precession period of $\sim 10^5$ yr comparable to estimated disc dispersal times (Shu et al. 1993).

Finally, the presence of the brown dwarf Gliese 229B with mass $\sim 45 M_J$ in a binary system indicates the potential existence of a separate population, at the one percent incidence level, of brown dwarfs (Oppenheimer et al. 2000) which could form from discs. The simulations presented here indicate eccentricity excitation due to the effects of the 1:3 resonance plays a role for these masses. The different type of disc behaviour could result in a distinct orbital and mass distribution for these objects as compared to extrasolar planets.

Acknowledgements. This work was supported by PPARC grant number PPARC GR/L 39094. It was also supported in part (F.M.) by the European Commission under contract number ERBFMRX-CT98-0195 (TMR network ‘‘Accretion onto black holes, compact stars and protostars’’). We thank Udo Ziegler for making a FORTRAN Version of his code NIRVANA publicly available. The calculations reported here were carried out using GRAND, a high performance computing facility funded by PPARC.

References

- Artymowicz, P. 1992, *PASP*, 104, 769
 Artymowicz, P. 1993, *ApJ*, 419, 155
 Artymowicz, P., & Lubow, S. H. 1994, *ApJ*, 421, 651
 Balbus, S. A., & Hawley, J. F. 1991, *ApJ*, 376, 214
 Balbus, S. A., & Hawley, J. F. 1998, *Rev. Mod. Phys.*, 70, 1
 Begelman, M. C., Blandford, R. D., & Rees, M. J. 1980, *Nature*, 287, 307
 Brouwer, D., & Clemence, G. M. 1961, *Methods of Celestial Mechanics* (New York, Academic press)
 Bryden, G., Chen, X., Lin, D. N. C., Nelson, R. P., & Papaloizou, J. C. B. 1999, *ApJ*, 514, 344
 Goldreich, P., & Tremaine, S. 1978, *Icarus*, 34, 227
 Goldreich, P., & Tremaine, S. 1980, *ApJ*, 241, 425
 Goodman, J., & Ryu, D. 1992, *ApJ*, 388, 438
 Hirose, M., & Osaki, Y. 1990, *PASJ*, 42, 135
 Ivanov, P. B., Papaloizou, J. C. B., & Polnarev, A. G. 1999, *MNRAS*, 307, 79
 Jeffreys, H. 1961, *MNRAS*, 122, 239
 Kato, S. 1978, *MNRAS*, 185, 629
 Kley, W. 1989, *A&A*, 208, 98
 Kley, W. 1998, *A&A*, 338, L37
 Kley, W. 1999, *MNRAS*, 303, 696
 Larwood, J. D., & Papaloizou, J. C. B. 1997, *MNRAS*, 285, 288
 Lin, C. C., & Shu, F. H. 1964, *ApJ*, 140, 646
 Lin, D. N. C., & Papaloizou, J. C. B. 1979, *MNRAS*, 188, 191
 Lin, D. N. C., & Papaloizou, J. C. B. 1986, *ApJ*, 309, 846
 Lin, D. N. C., & Papaloizou, J. C. B. 1993a, *Protostars and Planets III*, 749
 Lin, D. N. C., & Papaloizou, J. C. B. 1993b, *ApJ*, 416, 689
 Lubow, S. H. 1991, *ApJ*, 381, 259
 Lubow, S. H., Seibert, M., & Artymowicz, P. 1999, *ApJ*, 526, 1001
 Marcy, G. W., & Butler, R. P. 1998, *ARA&A*, 36
 Marcy, G. W., & Butler, R. P. 2000, *PASP*, 112, 137
 Masset, F. S. 2000, *A&A*, 141, 165
 Nelson, R. P., Papaloizou, J. C. B., Masset, F. S., & Kley, W. 2000, *MNRAS*, 318, 18
 Oppenheimer, B. R., Kulkarni, S. R., & Stauffer, J. R. 2000, To appear in *Protostars and Planets IV*, Tucson, AZ (University of Arizona Press)
 Papaloizou, J. C. B., & Terquem, C. 1995, *MNRAS*, 274, 987
 Papaloizou, J. C. B., & Lin, D. N. C. 1988, *ApJ*, 331, 838
 Papaloizou, J. C. B., & Terquem, C. 1999, *ApJ*, 521, 823
 Shakura, N. I., & Sunyaev, R. A. 1973, *A&A*, 24, 337
 Shu, F., Johnstone, D., & Hollenbach, D. 1993, *Icarus*, 106, 92
 Van Leer, B. 1977, *J. Comp. Phys.*, 23, 276
 Ward, W. R., Columbo, G., & Franklin, F. A. 1976, *Icarus*, 28, 441
 Ward, W. R., & Hahn, J. M. 2000, To appear in *Protostars and Planets IV*, Tucson, AZ (University of Arizona Press)
 Whitehurst, R. 1988, *MNRAS*, 232, 35
 Ziegler, U., & Yorke, H. W. 1997, *Comp. Phys. Comp.*, 101, 54